The Influence of Solidification Conditions on the Quality of Remelting Electrodes

Presenter:

Dipl.-Ing. Johannes Morscheiser

Studied metallurgy and materials science from 2003 to 2008 at RWTH Aachen University
Since 2008 he works as scientific engineer at IME Process Metallurgy and Metal Recycling, RWTH Aachen University, where he is currently doing his doctorate

The Influence of Solidification Conditions on the Quality of Remelting Electrodes

Dipl.-Ing. J. Morscheiser, M.Sc. P. Kontis, Prof. Dr.-Ing. B. Friedrich

IME Process Metallurgy and Metal Recycling, RWTH Aachen University
Intzestrasse 3, 52062 Aachen, Germany

Keywords: vacuum induction melting, solidification, segregation, alloy 718, laser induced breakdown spectroscopy

1 Abstract

Commonly, in the production of nickel-based superalloys a remelting step follows primary vacuum induction melting (VIM). The remelting is usually carried out via electroslag remelting (ESR) or vacuum arc remelting (VAR) and improves the cleanliness, the compactness and to a certain extent the homogeneity of the metal. For selected highly stressed rotating components, even the combination of all three processes to the so-called triple melt route (VIM-ESR-VAR) is compulsory.

Besides a thorough control of the remelting processes, a good electrode quality is essential to ensure the production of a defect-free and homogeneous ingot. Especially the VAR-process is prone to the presence of imperfections in the electrode like radial cracks or an extensive cavity pipe. The former can lead to undesired melt rate excursions, the latter to the formation of dendritic white spots, especially if the shrinking pipe contains dendrite clusters that can fall into the melt and sink to the bottom of the pool without melting. In the production of alloys that are susceptible to segregation, the attention has additionally to be turned to the homogeneous distribution of the alloying elements. The remelting processes are known to reduce microsegregation and radial macrosegregation, but as in the processes only a small volume of the metal is molten at a time, there is no possibility given to remove severe segregation over the height of the primary ingot that occurred during solidification.

As the structure of casting ingots strongly depends on the cooling rate during solidification, an investigation was carried out at IME, RWTH Aachen University to identify the potential of water-cooled copper as mould material for the production of nickel-based superalloys instead of commonly used grey cast iron moulds. Therefore, alloy 718 was cast into both mould types under the exact same conditions (casting temperature, pressure, pouring rate). To reveal the degree of macrosegregation, the produced ingots were cut longitudinally and the cross section was analysed by laser-induced breakdown spectroscopy (LIBS). Thus, for each sample, a distribution map with a high spatial resolution was created for the major alloying elements and niobium in particular, as this element is known for its tendency to segregate intensely. Additionally, radial samples were afterwards metallographically prepared and analysed via light microscopy to determine the secondary dendrite arm spacing. Hereby, the local solidification time was calculated for the respective positions in the

ingot and correlated with the chemical composition to quantify the effect of the cooling rate on the degree of segregation. In addition, the structure of the cavity pipe was determined concerning its magnitude on the one hand and its surface morphology on the other hand and evaluated concerning possible sources for defects in remelting ingots.

This paper presents the results of the described investigations and gives an outlook on a possible use of water-cooled copper moulds in the production of nickel-based superalloys with regard to electrode quality, practicality and safety issues.

2 Introduction

The production of nickel-based superalloys is based on a combination of complex processes that are supposed to ensure a high quality of the final product. The manufacturing route commonly comprises primary melting in a (vacuum) induction or electric arc furnace, which is followed by at least one remelting step in an electroslag or vacuum arc remelting furnace. For exceptionally stressed parts like turbine discs, even multiple remelting steps are applied to minimize the probability of defects in the material. Here, the variant VIM-ESR-VAR, the so-called *triple-melt* route, is the most common combination. The so produced ingots mostly undergo an intense heat treatment before they are brought into their final shape by metal forming and machining.

This paper concentrates on the casting and solidification of consumable electrodes by VIM for subsequent remelting processes, as a good quality of the electrode is essential for constant remelting conditions and therefore homogenous material properties in the resulting ingot. Especially the VAR process is very susceptible for imperfections in the utilized electrodes as will be described in the following.

3 Fundamentals

The central objectives of remelting processes are the refinement of the consumable electrode with regard to solved impurities and non-metallic inclusions as well as the controlled solidification of the liquid metal. The latter is supposed to generate a uniform solidification structure without porosity, shrinking cavities and irregularities in the microstructure. For this purpose it is crucial to keep the melting and solidification conditions as constant as possible, what is mostly achieved by the control of the melt rate and the distance between the electrode and the liquid metal pool. As the melt rate is interrelated to the current density at the electrode tip, changes in the cross-section of the electrode directly lead to anomalies in the melt rate. A major source of such changes is the existence of shrinking cavities in the electrode, which is why the electrode should be as dense as possible. Especially vacuum arc remelting is prone to anomalies in the electrode, as the heat balance of this process is more fragile in comparison to ESR. While in ESR the slag bath forms a local heat reservoir that can compensate for certain changes in the electrode, in VAR even minor variations in the constitution of the electrode can cause significant fluctuations in the heat balance of the process and therefore in the solidification structure of the ingot as well. Hence, in

VAR, electrodes that were produced virtually free of porosities or cavities by the ESR process show significant advantages in comparison to VIM electrodes. [1] The formation of an extensive shrinkage pipe can hardly be influenced by simple measures like the variation of the mould temperature but only by techniques like the use of mould powder, feeders, uphill casting or different mould designs. However, not only the size of the void but also its surface morphology affects the quality of the remelting ingot, as protruding metal needles in sizes of several millimetres can fall into the metal pool and cause so-called dendritic white spots if the needles are not fully dissolved in the liquid metal pool. [2]

Another possible source of inhomogeneities in the ingot is the presence of transversal cracks in the electrode, as they adversely affect the heat transfer to the cold zones of the electrode. Below the crack, the heat accumulates while the area above the crack remains at comparably low temperatures. That leads to a temporary increase of the melt rate, which is followed by a sudden decrease before a steady state is reached again. Mir et al. [3] calculated the influence of transversal cracks on the melt rate and the diagram in Figure 1 illustrates their findings for the three different configurations of cracks that are given in the sketch right to the diagram.

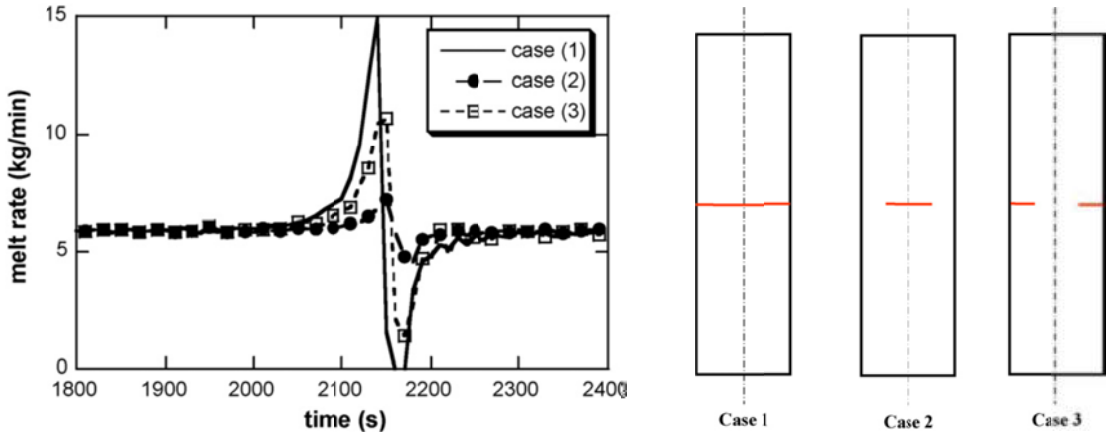

Figure 1: Calculated behaviour of the melt rate during VAR in case of transversal cracks in the electrode [3]

A possible source for the formation of cracks in the electrodes is the presence of large Laves phase clusters in the electrode. When the internal stresses in the metal increase during solidification of the ingot or the heating-up while remelting, larger particles or clusters of Laves phase can act as preferential sites for crack initiation due to their inherent brittle nature. Therefore, it is advisable to keep the amount of Laves phase in the electrodes as low as possible. As according to Figure 2 the fraction of Laves phase in alloy 718 depends on the cooling rate during solidification, a fast solidification of the ingot should have a beneficial effect on the electrode quality with regard to the amount of Laves phase.

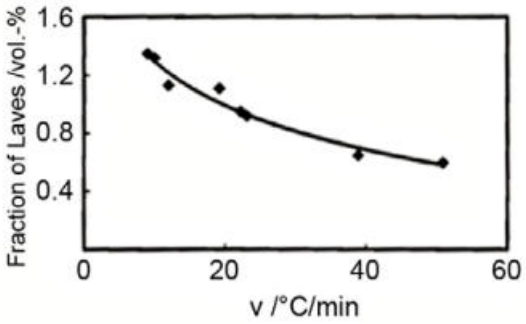

Figure 2: The effect of the solidification cooling rate on the volume fraction of the Laves phase in alloy 718 [5]

For evaluation of the solidification cooling rate in as-cast material, the determination of the secondary dendrite arm spacing (SDAS) is well established. According to Patel and Murty [4], the interrelationship between both values in alloy 718 is presented by equation 1, where SDAS is given in μm:

$$SDAS = C \cdot \left(\frac{T_l - T_e}{\dot{T}}\right) \quad (1)$$

C: a constant, for alloy 718 about 10; T_l: liquidus temperature; T_e: eutectic temperature (γ/Laves); $\dot{T}$: cooling rate (°C/s)

As the value of the constant depends on the composition of the cast material, in literature often only the SDAS is employed for the characterisation of the solidification structure.

4 Experimental Investigation

Two electrodes of alloy 718 were produced by vacuum induction melting and cast into a mould of grey cast iron and a water-cooled copper mould respectively. The resulting ingots were characterised by light and scanning electron microscopy as well as different methods of chemical analyses.

4.1 Melting and Casting/Manufacturing of Electrodes

The melting and casting of both ingots was carried out in a 150 kW-vacuum induction furnace at IME under identical, industry-oriented conditions except for the mould material. The charges were made up of revert material from the same master batch and their chemical composition corresponded to the specification of alloy 718 according to AMS 5562 given in Table 1.

Table 1: Specification limits for the major alloying elements in alloy 718 according to AMS 5562 (in wt.-%)

Element	Ni	Cr	Fe	Mo	Nb	Al	Ti
Lower specification limit	50	17	Balance	2,8	4,75	0,2	0,65
Upper specification limit	55	21	Balance	3,3	5,5	0,8	1,15

At the beginning of each trial, the furnace was evacuated below 0.01 mbar before power was applied to the induction coil. As refractory, an alumina-based crucible came into operation. After the whole charge was molten and homogenised, vacuum degassing took place for approximately 20 minutes before the pressure was adjusted to 250 mbar of argon. To ensure the correctness of the chemical composition, samples were taken from the liquid melt and analysed by x-ray fluorescence spectroscopy. Just before casting, Ca and Mg were added to the melt in the form of nickel-based master alloys to adjust the sulphur content to non-critical values. To guarantee comparable casting conditions, the temperature was regulated to 1420°C and the pouring rate to 2.5 – 3.0 kg per second.

As the main aim of the present investigation is the characterization of the influence of the cooling conditions on the quality of the produced ingot, a water-cooled copper mould and a conventional grey cast mould were used for casting. The inner dimensions of both moulds were 900 mm in length and approximately 110 mm in diameter, with the difference that the copper mould was cylindrical whereas the iron mould was slightly tapered. While the latter was made from one single piece, the copper mould consists of two half-shells that are held together by massive steel clamps (Figure 3, centre). The design of the cooling channels that lead the water through the mould is illustrated in Figure 3, left. The water flow rate through the mould was set to 21.5 litres per minute with an inlet temperature of ca. 8°C.

The general set-up of the casting is given in Figure 3, right, showing the cross-section of the furnace with the vacuum chamber, the induction coil that contains the crucible and the refractory backing, the casting funnel and the mould. Through a vacuum sealing in the lid, thermocouples as well as charging and sampling devices can be lowered into the furnace without influencing the atmosphere in the vacuum chamber.

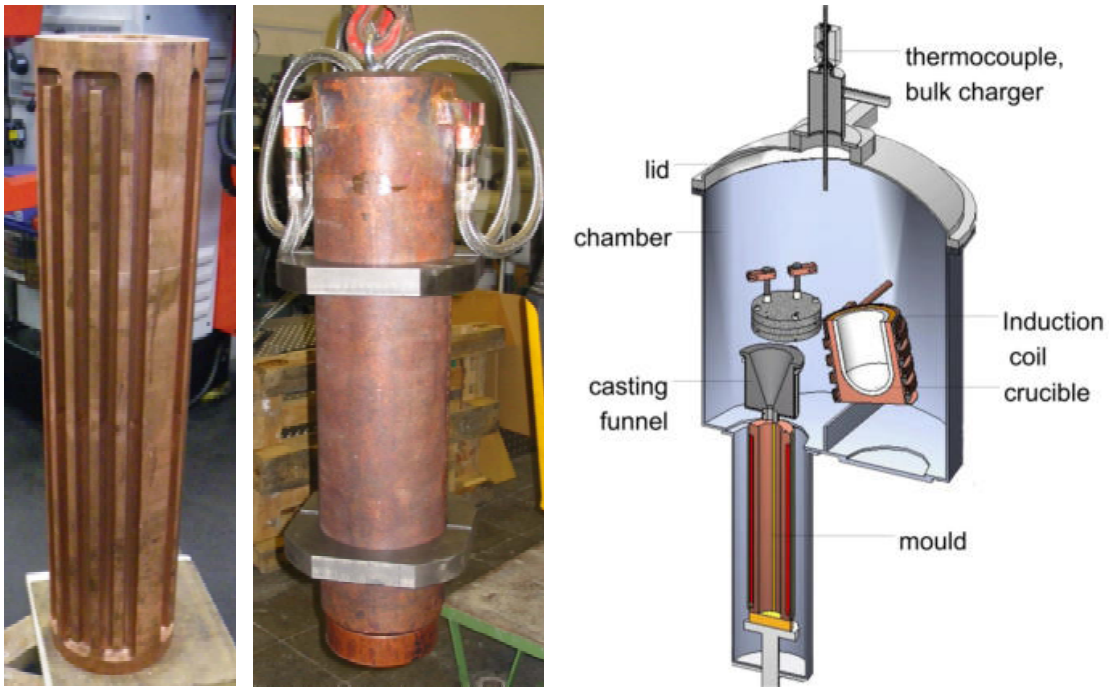

Figure 3: Left: cooling channels in the water-cooled copper mould; centre: the water-cooled copper mould; right: cross-section of the casting set-up

4.2 Sampling and Analyses

The produced ingots were between 59.8 and 60.6 kg in weight and reached between 82.4 and 84 cm in length. As a first step, both ingots were cut longitudinally with a band saw. The resulting cross section was then evaluated by sight with regard to the size and the surface morphology of the casting void. Here, particular attention was paid to the possible presence of protruding crystals and needles that might be a possible source for white spots during vacuum arc remelting.

For the evaluation of the material's microstructure, radial, semi-circular slices were taken from different heights in the ingots according to Figure 4, left, where CO stands for the ingot from the water-cooled copper mould and GC for the one from the grey cast iron mould. From these slices, a bar was cut, which was then halved, embedded and metallographically prepared (Figure 4, bottom right). The resulting samples were first analysed by light microscopy to investigate the general microstructure and to determine the secondary dendrite arm spacing as a function of the position in the ingot. For the latter, the distance between the edge and the centre of the ingot was split into eight measuring zones of equal size, and in each zone, at least four dendrites were measured. For this purpose, the length of a dendrite was determined and divided by the number of present secondary dendrite arms as shown in Figure 4, top right.

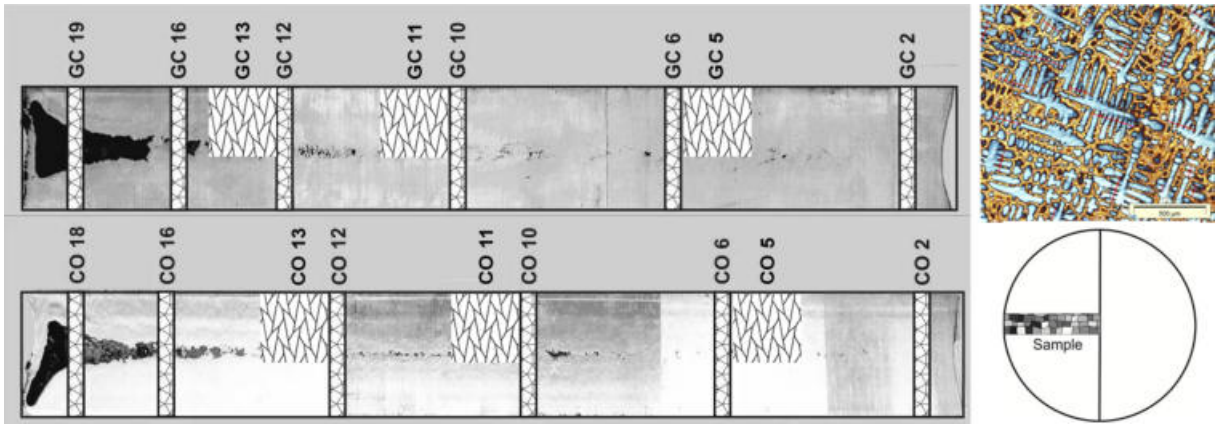

Figure 4: Positions of the samples in the ingots and determination of the secondary dendrite arm spacing (top right)

From the samples that were used for microstructural analysis by light microscopy, the slices 6, 10 and 16 were also investigated by scanning electron microscopy with energy dispersive x-ray analysis (SEM-EDX) to determine the amount, the size and the composition of the existing phases.

Apart from the structural analysis of the ingots, an extensive chemical analysis of the material was carried out. It was mainly focused on the identification of micro- and macrosegregation, in particular with regard to niobium, as the latter is known to be one of the elements that segregate most in alloy 718. In a first approach, the whole longitudinal cross section of the ingots was analysed by laser induced breakdown spectroscopy (LIBS) with a lateral resolution of $\Delta x / \Delta y = 1$ mm (Figure 5, left). The wavelength ranged from 200 to 780 nm so that several elements like Ti, Fe, Cr, Ni and Nb could be detected at the same time. As the size of the measured spots was only around 20 microns each and therefore in the range of typical microsegregation

patterns, this method of analysis turned out to be inapplicable for the identification of macrosegregation. To further enhance the accuracy of the measurements, slices of 70 x 70 x 10 mm were cut from the ingots in three different heights and analysed in a closed LIBS unit under argon to negate the influence of the atmosphere. The position of these square slices is marked in Figure 4 as CO respectively GC 5, 11 and 13. Furthermore, the lateral resolution was increased to step sizes of 20 microns in x- and 100 microns in y-direction. In the current investigation, an area of 50 x 10 mm was analysed in order to identify fluctuations in the niobium distribution as a function of the distance to the surface of the ingot. The measured areas can be seen as dark bars on the photo in Figure 5, right. Due to technical restrictions of the LIBS unit, a 7 mm wide stripe near the edge of each sample could not be analysed. As the spectrometer was not calibrated for alloy 718 in particular, the results of the measurements will only be presented qualitatively by the measured intensity. However, this method facilitates the determination of the niobium distribution in different samples and allows for a comparison of the degree of segregation between both ingots.

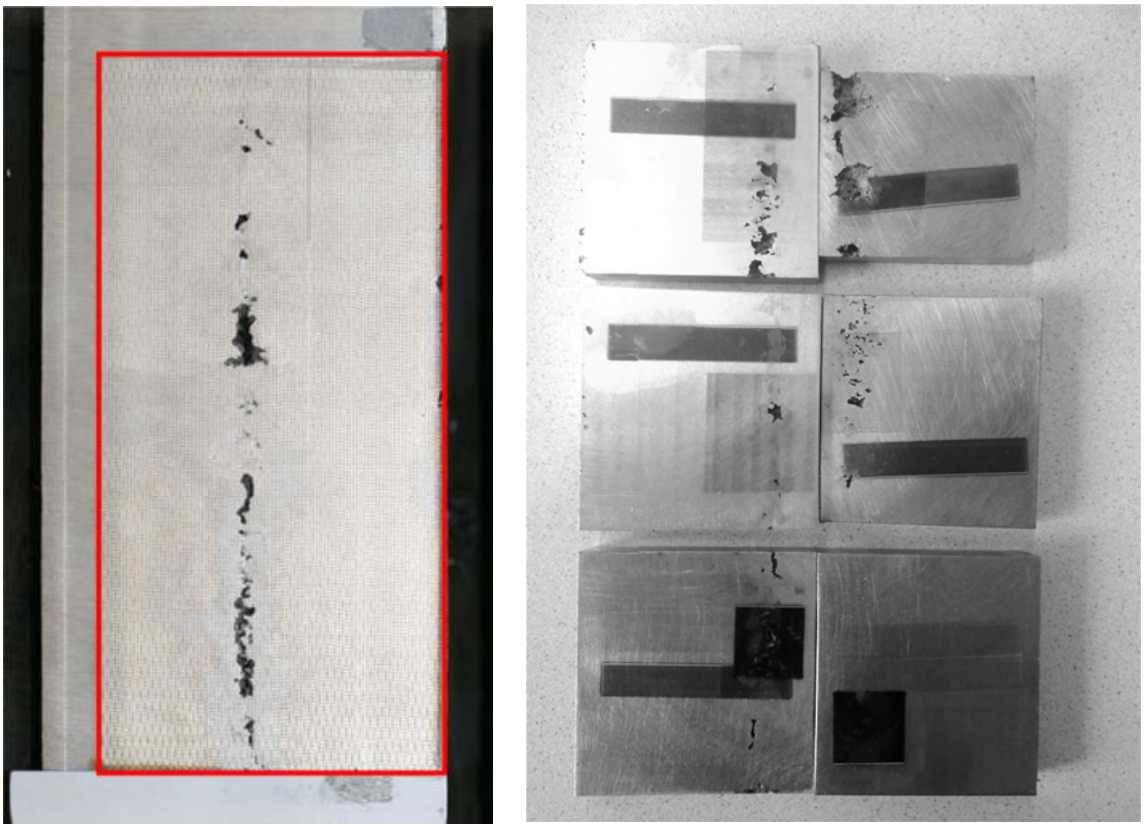

Figure 5: Exemplary images of the measured LIBS samples

To obtain the absolute niobium content for selected samples and to support the measurements made by LIBS, quantitative SEM-EDX measurements in dendritic and interdendritic areas were carried out. The utilized scanning electron microscope was a Jeol6380LV, which was equipped with an Oxford Inca 7582 EDX device.

To obtain information about the macroscopic distribution of niobium, the samples 5, 11 and 13 were additionally analysed by spark optical emission spectroscopy (OES) and glow discharge (GD) OES in three different distances between the surface and the centre of the ingot. The measurements were carried out by a Spectro MAXx spark OES unit and the analysed area was approximately 19.6 mm² per

measurement, so that the effect of microsegregation on the results should have been negligible. The GD-OES was a GDA750 from Spectruma Analytik GmbH and the analysed area was 12.6 mm² at a time.

5 Results and Interpretation

5.1 Macroscopic Appearance of the Ingots

As could already be noted in Figure 4, the shape and size of the macroscopic casting voids look very similar in both ingots. Besides the size, the surface morphology of the casting void is an important criterion for the evaluation of the electrode quality, as protruding or loose metallic needles can cause dendritic white spots as described in paragraph 3. As can be seen in the following Figure 6, the upper part of the casting void has a smooth surface in both ingots. However, as can be seen in the close-ups of the casting voids, the morphology of the lower part is significantly more uneven in the water-cooled copper mould and the protruding metal tips can be counted as potential source for fall in and the causation of white spots. That leads to the conclusion, that the water-cooled mould rather adversely affects the surface morphology of the casting void.

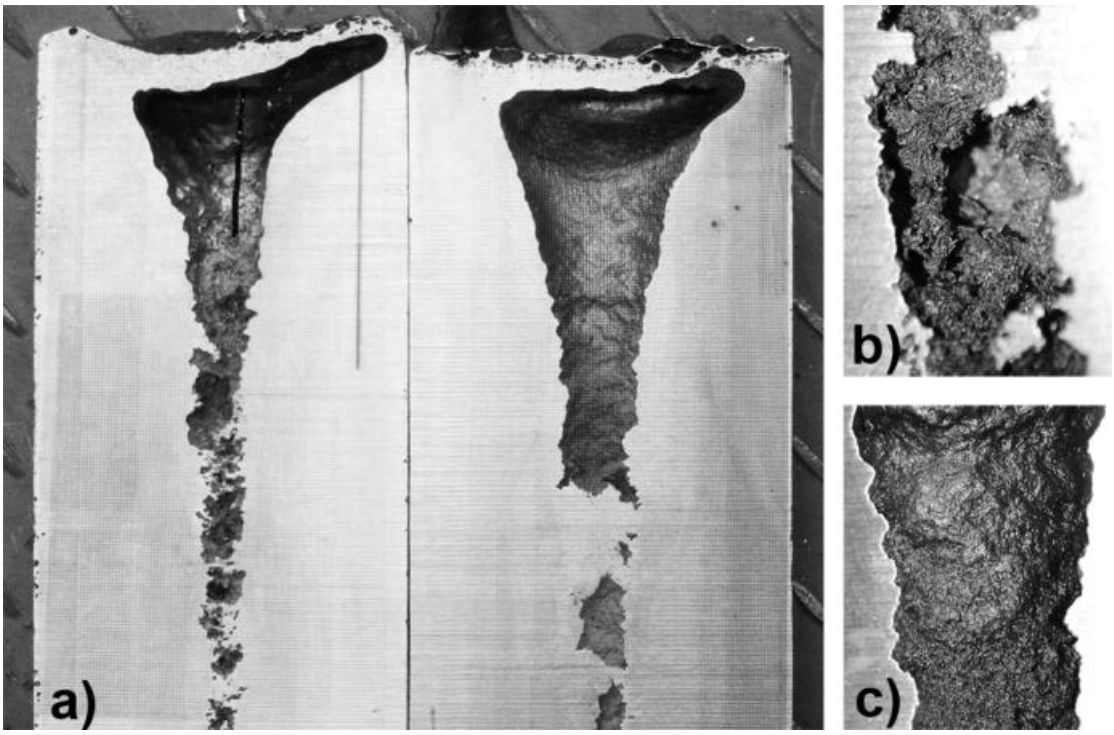

Figure 6: a) Shrinkage cavities in the ingots from the water-cooled copper mould (left) and the grey cast iron mould (right)
b) Close-up of the cavity in the ingot from the water-cooled mould
c) Close-up of the cavity in the ingot from the grey cast iron mould

5.2 Microstructural Analyses

5.2.1 Light Microscopy

Figure 7 presents the results of the SDAS measurements as a function of the distance from the ingot surface. It is evident, that the SDAS is smallest in the outer parts of both ingots and increases to the centre. The minimum spacings were measured in the water-cooled ingot with 9 to 15 µm, whereas the smallest spacings in the ingot from the grey cast iron mould were 15 to 25 µm. In both ingots, the SDAS in the central part was between 25 and 35 µm except in the sample CO2. There, a significant drop to approximately 10 to 13 µm could be detected in the inner part of the ingot. To a certain extent, this effect is presumably caused by the multidimensional heat transfer not only to the walls but also to the base plate of the mould. However, no logical explanation could be found why this rapid decrease happens just at the mid-radius. In the grey cast iron mould, the influence of the base plate is not as evident as in the water-cooled copper mould but the smallest SDAS were measured in the lowest sample as well.

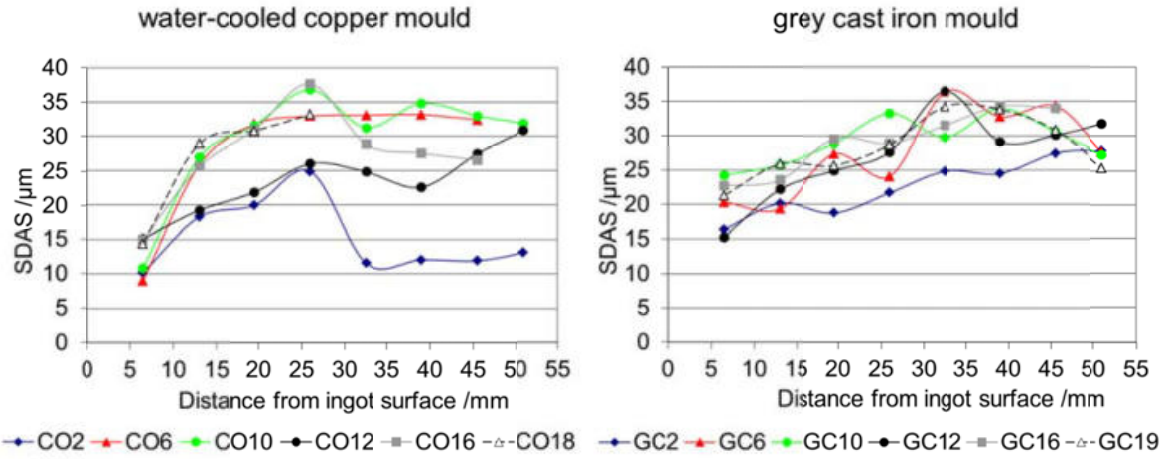

Figure 7: Results of the SDAS measurements

The fact, that the SDAS in the outer layer of the ingot is smaller in the water-cooled copper mould, accounts for a faster heat extraction in comparison to the grey cast iron mould. As copper has a high thermal conductivity and the water flow supports the heat transport, this was to be expected. However, already 15 mm from the surface the SDAS of both ingots lies in the same range. To a certain extent, the influence of the water-cooling might be negated by the circumstance that in the solid-state heat is only transported by conduction and not by convection as in the liquid, and that the thermal conductivity of solid alloy 718 rapidly decreases with decreasing temperature. Nevertheless, the effect of the thermal contraction during solidification and the resulting gap between the ingot and the mould is assumed to have a greater influence on the heat extraction from the metal, as the thermal conductivity of argon is negligible and the bigger part of the heat has to be transferred to the mould by radiation.

The observation, that the water-cooled mould primarily affects the solidification in the surface-near part of the ingots, could be verified by the general evaluation of the microstructure. Near the surface of the ingot from the water-cooled mould, there is an almost unidirectional dendritic microstructure as can be seen in Figure 8, left, whereas for the orientation of the dendrites in the other ingot no predominant direction of growth could be detected. However, in the central part of both ingots the structure looks alike as will be also showed in the evaluation of the SEM analysis.

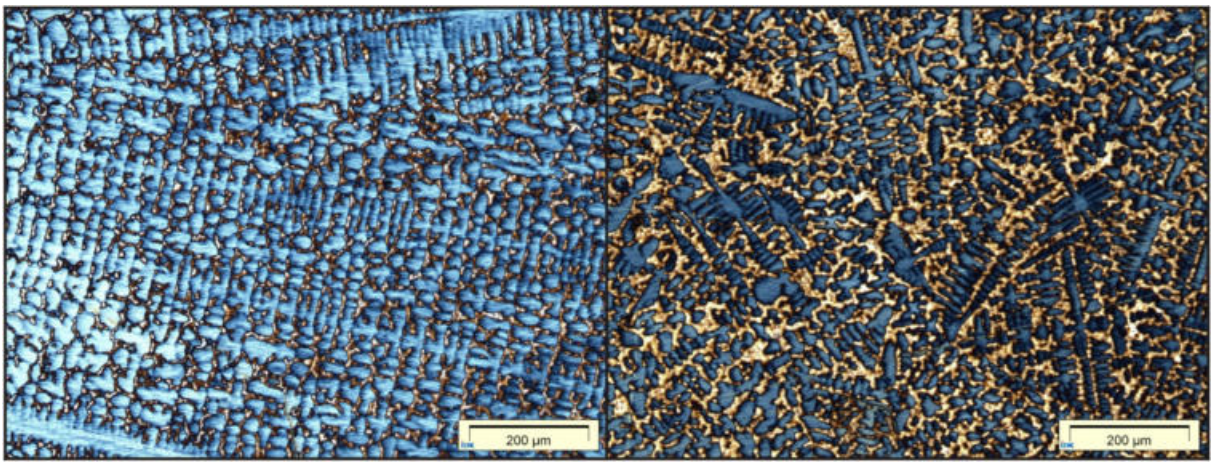

Figure 8: Characteristic image of the microstructure in the surface near area in ingots from a water-cooled copper mould (left) and a grey cast iron mould (right)

5.2.2 SEM

As described in paragraph 4.2, the samples 6, 10 and 16 from each ingot were additionally analysed by SEM-EDX. On each sample, four areas were examined between the surface and the centre of the ingot. In the following, they are denominated from 1 (surface-near) to 4 (centre). As the utilization of EDX allowed an identification of particular phases and the determination of the local composition at selected spots, it was possible to obtain additional information with regard to the formation of phases and to the degree of segregation.

As in the light-microscopical investigation, the most significant difference between both ingots with regard to the formation of specific phases could be identified in the surface-near area. The upper half of Figure 9 shows SEM images of the samples CO10 (left) and GC10 (right), where the primary dendrites can be seen as dark areas that are surrounded by the brighter interdendritic domains in which the precipitated phases are located. The lower half shows the same images with an increased level of contrast, what allows an easier analysis of the distribution of the precipitates.

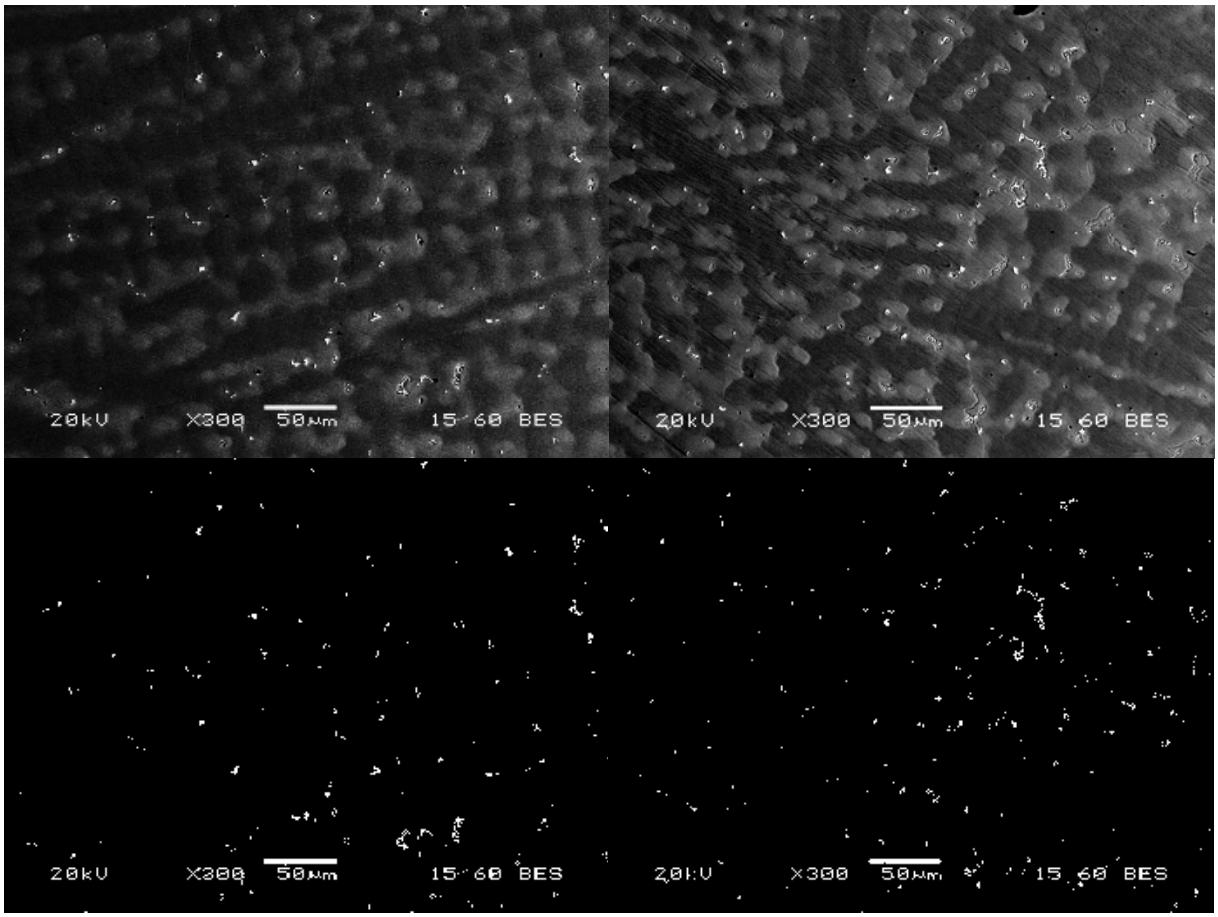

Figure 9: SEM image of area 1 in the samples CO10 (left) and GC10 (right) with standard (top) and increased (bottom) contrast levels

A quantitative image analysis indicates that the total area of precipitates in the right picture is more than twice as large as in the left image. It is also observable, that the maximum size of the precipitated phases is smaller in the almost unidirectional dendritic microstructure, what is considerably owed to the higher cooling rates: On the one hand, due to the parallel orientation of the primary dendrites and the comparably small SDAS, the average interdendritic domains are smaller and therefore the room for the development of precipitations is restricted. On the other hand, the formation of precipitates often depends on a local increase of alloying elements due to segregation effects and the fast solidification suppresses the latter to a certain extent.

Moreover, not only the size and the amount of precipitates differ between the ingots but also the type of the precipitated phases. The following Figure 10 presents characteristic SEM images from area 2 in the samples CO6 (left) and GC6 (right) and it is clearly observable, that the left image predominantly shows greyish precipitates, which were identified as Nb-containing carbides, whereas the white precipitates in the right image consist of Laves phase. This is in good accordance with the findings of Dong et al [6], who stated that the formation of Laves phase in alloy 718 increases with the local solidification time. As the latter is comparably short in the surface-near volume of the ingot from the water-cooled mould, it explains the low amount of Laves phase.

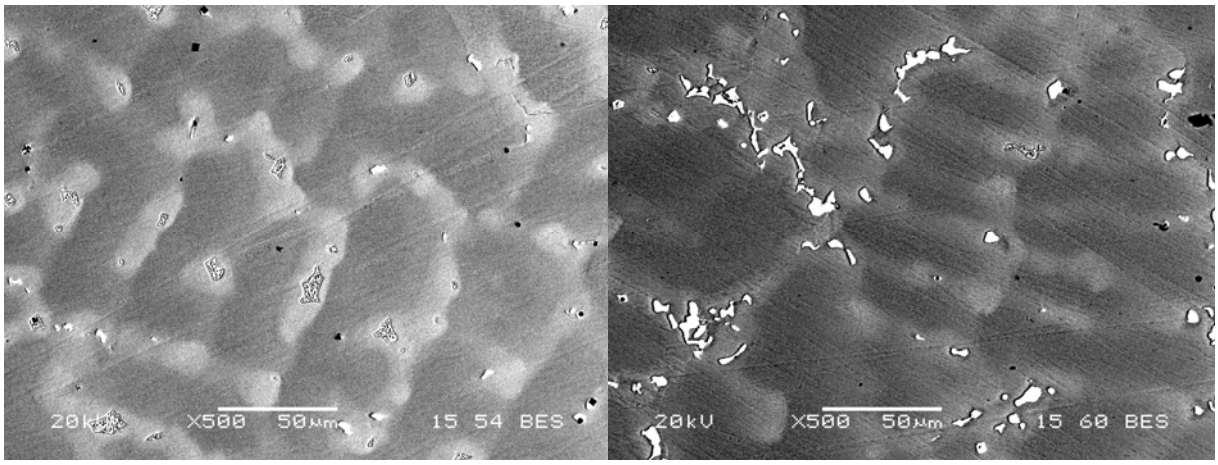

Figure 10: SEM image of area 2 in the samples CO6 (left) and GC6 (right)

However, the positive effect of the water-cooling on the suppression of the Laves phase is only present in the outer part of the ingot what also conforms to the results from the SDAS measurements. As a characteristic example for the central part of the ingot, Figure 11 illustrates that the amount of Laves phase is nearly the same in area 3 in the samples CO16 (left) and GC16 (right). Here, Laves phase can be found in nearly every interdendritic domain, what is supposedly caused by the increased local solidification times.

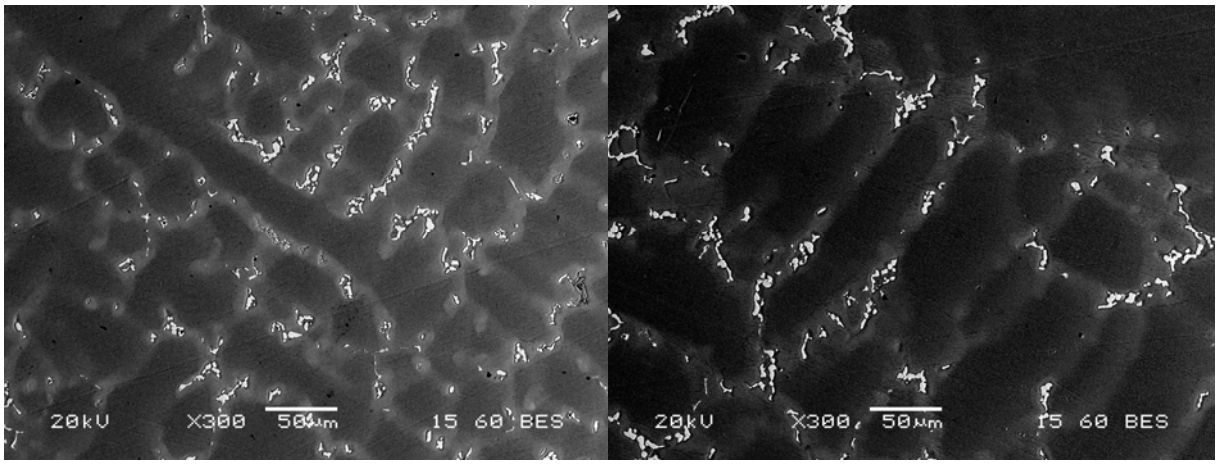

Figure 11: SEM image of area 3 in the samples CO16 (left) and GC16 (right)

5.3 Outcome of the Chemical Analyses

5.3.1 SEM-EDX

As the following Figure 12 depicts, the EDX measurements of selected areas in both ingots showed a significant difference in the niobium distribution between the dendritic and the interdendritic area. In both ingots, the primary dendrites are depleted in niobium whereas the interdendritic area is enriched in this element. While the average niobium level in the dendrites is at 2.88 wt.-% respectively 2.87 wt.-%, the average content in the interdendritic area is 8.48 wt.-% in both ingots.

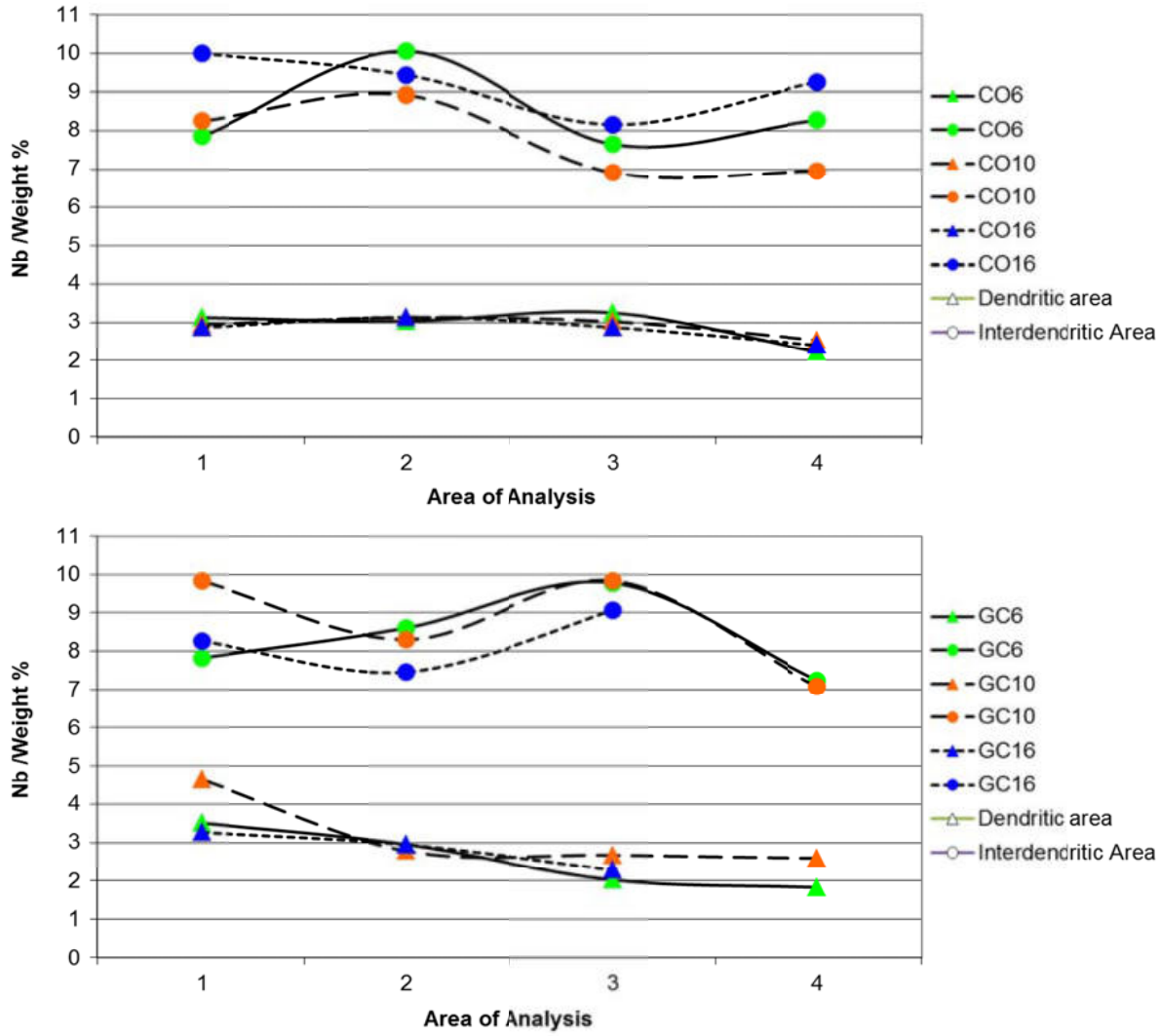

Figure 12: Results of the EDX analyses (top: ingot CO, bottom: ingot GC)

The calculation of the partition coefficient for Nb according to the definition in equation 2 given by Knorovsky et al. [7] results in 2.94 for the ingot from the water-cooled mould and 2.96 for the ingot from the grey cast iron mould.

$$p = \frac{\text{concentration in the interdendritic area}}{\text{concentration in the dendritic area}} \qquad (2)$$

p: partition coefficient

The partition coefficient is a measure for the partition of an element to different phases within an alloy. As Table 2 illustrates, the determined values are in good accordance to the findings of previous experimental investigations.

Table 2: Experimentally determined partition coefficients for Nb in alloy 718

Reference	Present study	Knorovsky [7]	Yang [8]	Dong [6]
Part. coeff. for Nb	2.94 – 2.96	2.4	2.04-3.91	3.41

While the niobium content in the primary dendrites slightly decreases from the surface to the centre in both ingots, the niobium concentration in the interdendritic area does not follow a clearly distinguishable trend. The characteristics of the graphs of the interdendritic area look nearly contrary to each other, but so far, no suitable explanation was found for this circumstance.

5.3.2 LIBS

The following Figure 13Figure 13 illustrates the distribution of niobium according to the analysis by laser-induced breakdown spectroscopy. The diagrams on the left hand side show the results for the ingot from the water-cooled copper mould for the samples CO5, CO11 and CO13 (from bottom to top) whereas the diagrams on the right hand side show the corresponding samples of the ingot from the grey cast iron mould. As described above, the absolute niobium concentration could not be determined with this method and therefore only the intensity of niobium is indicated in the images. Nevertheless, this still allows an overview over the local distribution of this element in the six samples. It must be noted, that the surface right to 48 mm in sample GC13 could not be measured due to a shrinkage cavity and therefore this area, which is mostly below an intensity of 230, needs to be excluded in the discussion of the diagrams. What is more, the green line marks the edge of areas in the interval between 1150 and 1380 to allow for an easier identification of these specific domains.

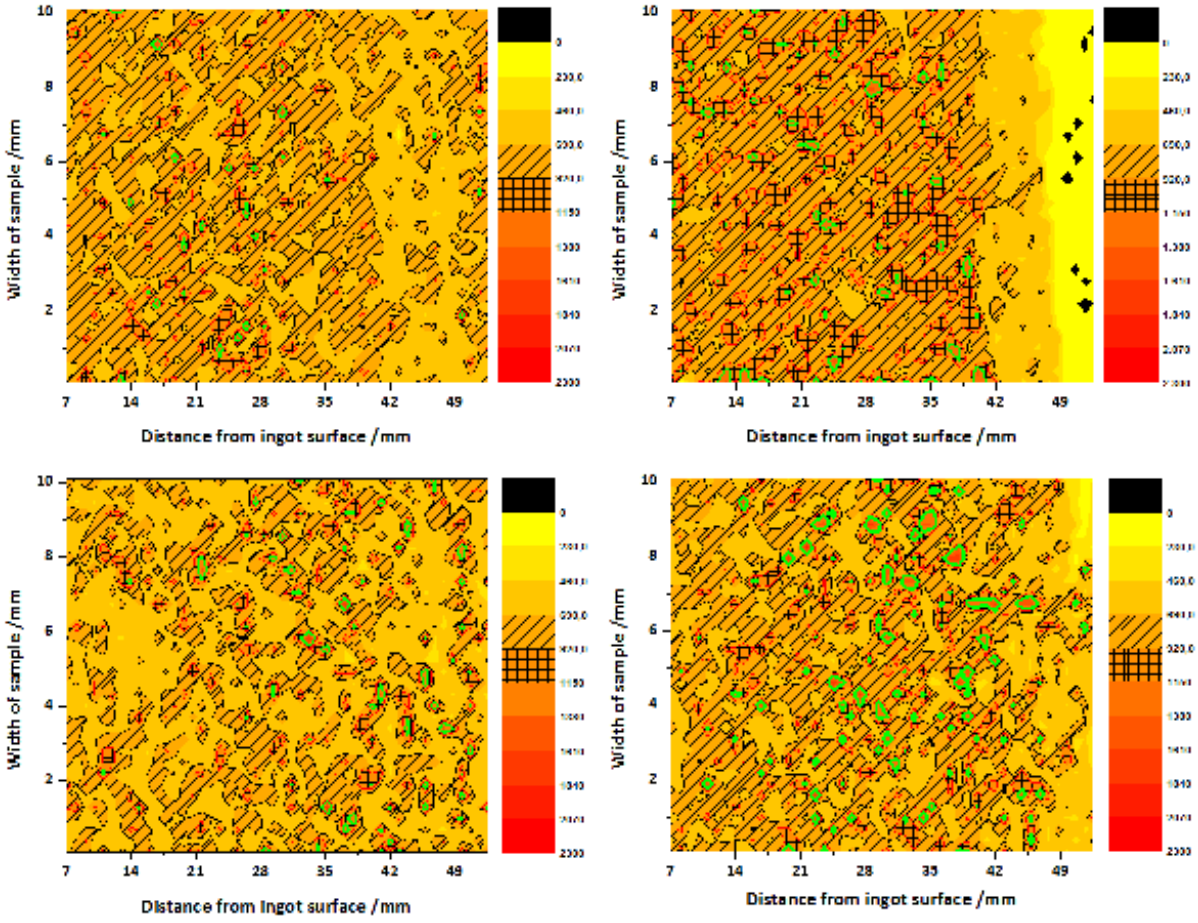

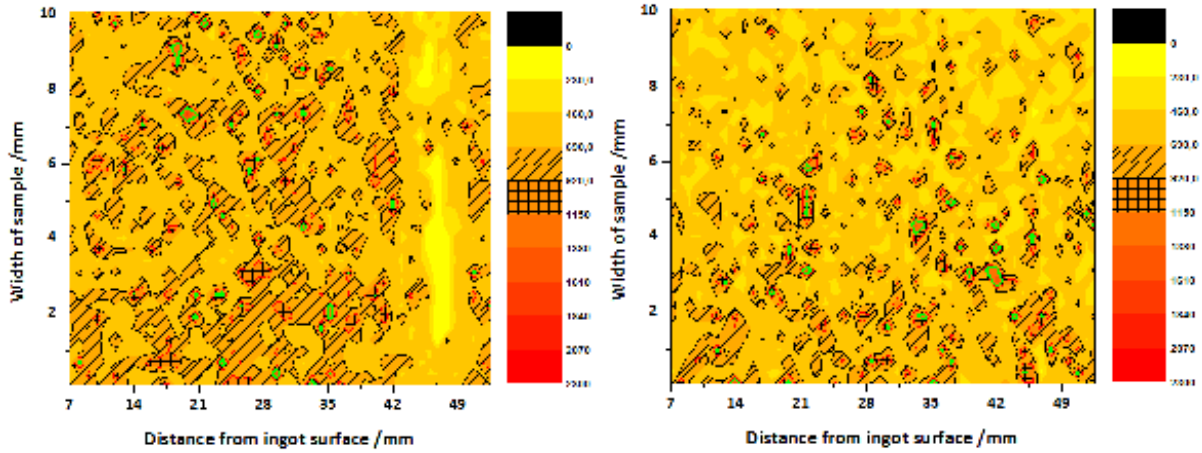

Figure 13: Local niobium distribution measured by LIBS: left: CO13, CO11, CO5, right: GC13, GC11, GC5 (from top to bottom)

It is observable that the total amount of niobium seems to increase with the height in the ingot. Whereas in the samples 5 the largest fraction of the area shows an intensity of 690 and lower, the average intensity in the samples 10 and 13 is shifted to considerably higher values. For a better illustration, Figure 14 depicts the accumulated number of measurements for each interval of intensity for the samples CO5 and CO13 and it is evident that in the second sample the number of spots with an intensity larger than 690 is increased at the expense of spots with lower intensity.

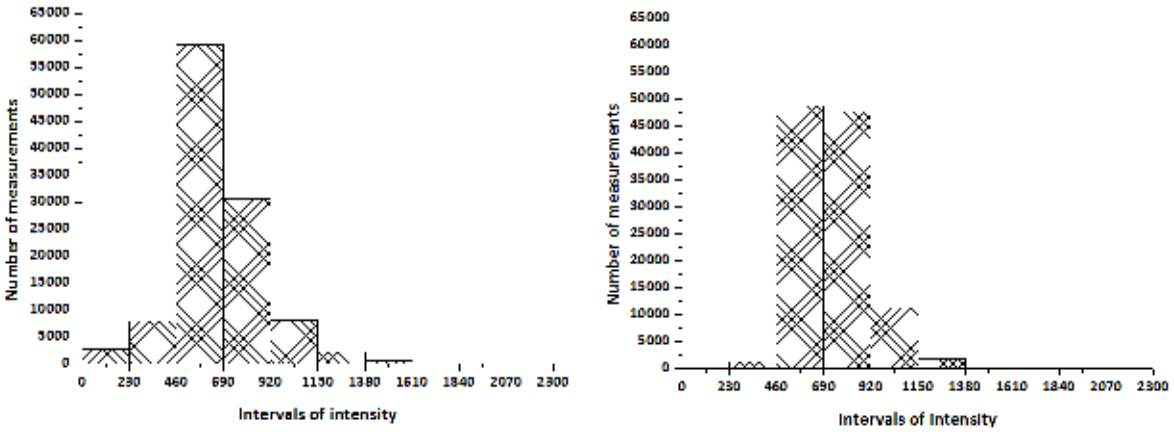

Figure 14: Accumulated number of measured spots for the respective intervals of intensity in LIBS for the samples CO5 (left) and CO13 (right)

A direct comparison of the samples CO11 and GC11 supports the findings from the SEM analysis with respect to the formation of Laves phase. Whereas in GC11 the areas with an intensity between 1150 and 1380 are almost uniformly spread over the analysed surface, in CO11 most of these niobium-rich clusters are located near the centre of the ingots. This corresponds quite well with the distribution of Laves phase that was determined by SEM analysis.

Furthermore, some samples seem to show an indistinct tendency to have lower niobium concentrations near the centre of the ingot. For instance, the intensities in the areas between 40 and 50 millimetres in the samples CO5, CO13 and GC11 and in the area left to the casting void in GC13 are generally lower than in the rest of the re-

spective samples. This is rather unexpected inasmuch as niobium is known to be rejected to the melt in alloy 718 and therefore it was assumed that the niobium concentration would be highest in the area that solidified last. For this effect, the established theorems described by Campbell [9] or Gottstein [10] do not present a satisfying explanation and further investigations have to be carried out to identify its source.

5.3.3 Spark OES & GD-OES

The investigation of the chemical composition by spark OES and GD-OES showed no significant fluctuation of the niobium content in both ingots on a macroscopic scale. All variation in the composition was within the measurement uncertainty of the two utilized analytical methods. As the size of the measured areas was rather large in comparison to LIBS, the effect of depletion in niobium near the centre of the ingots could not be verified on a macroscopical scale. In general, the results of the spark and GD-OES lead to the conclusion that in both moulds the heat extraction was sufficient to suppress the formation of significant macrosegregation effects.

6 Conclusions

The results of the various applied analyses indicate that the difference between electrodes that have been cast into a water-cooled copper mould and a grey cast iron mould, which was at ambient temperature, is rather insignificant. Neither could the formation of Laves phase be considerably suppressed by the faster cooling rates in the water-cooled mould nor did they have a substantial impact on segregation effects or the structure of the shrinking cavity. In the surface-near volume of the water-cooled ingot, an improvement of the characteristics with regard to the formation of Laves phase and smaller SDAS could be identified but this zone is too small to have significant impact concerning possible sources for defects in subsequent remelting steps.

Furthermore, the utilization of water-cooled moulds requires a high level of safety measures, as the presence of water in proximity to liquid metal always forms a high potential risk. In order to avoid catastrophic events, the mould must either be equipped with a reliable emergency water supply or it must be designed in such a way, that the amount of copper is able to absorb the heat that is contained in the melt. For the calculation of the latter, not only the thermal capacity of the metal but also the heat of fusion that is released during solidification must be regarded.

In general, the benefit of utilizing water-cooled copper moulds for the fabrication of remelting electrodes of nickel-based superalloys does not seem to outweigh the disadvantages such as higher cost and safety issues. However, the results of the current investigation need to be validated by further trials to increase the confidence level of the conclusions. Furthermore, the area that is investigated by LIBS needs to be extended to permit more precise analyses of the segregation behaviour. Especially the area directly near to the surface needs to be investigated more closely, what was not entirely possible in the current study due to the design of the specimen holder. In addition, an extensive calibration of the LIB-spectrometer would be desirable to obtain the absolute concentrations of the analysed elements.

7 Acknowledgements

We would like to thank the EU Erasmus Programme for financing the stay of M.Sc. Paraskevas Kontis in Aachen as well as his home university National Technical University of Athens and Assistant Professor George Fourlaris for supporting the current research project with SEM analyses.

8 References

[1] Moyer, J. M., et al.; Advances in Triple Melting Superalloys 718, 706, and 720; in: Superalloys 718, 625, 706 and various Derivatives, The Minerals, Metals & Materials Society, 1994, p. 39-48

[2] Jackman, L.A., Maurer, G.E., Widge, S.; White spots in superalloys; in: Superalloys 718, 625, 706 and various Derivatives, The Minerals, Metals & Materials Society, 1994, p. 153-166

[3] Mir, H.E., et al.; Thermal behaviour of the consumable electrode in the vacuum arc remelting process; Journal of Materials Processing Technology 210 (2010) 564–572

[4] Patel, A.D., Murty, Y.V.; Effect of Cooling Rate on Microstructural Development of Alloy 718; in: Superalloys 718,625,706 and Various Derivatives, 2001, TMS, p.123-132

[5] Zhao,J., Yan, P.; The effect of cooling rate of solidification on microstructure and alloy element segregation of as-cast alloy 718; in: Superalloys 718,625,706 and Various Derivatives, 2001, TMS, p. 133-140

[6] Dong, Y.-W., Jiang, Z.-H., Li, Z.-B.; Segregation of Niobium during Electroslag Remelting Process; Journal of Iron and Steel Research, 2009, 16(1), p. 7-11

[7] Knorovsky, G.A., et al.; Inconel 718: A Solidification Diagram; Metallurgical Transactions A, Vol. 20A, October 1989, p. 2149-2158

[8] Yang, A.-M.; Study of Structure Refinement and Optimization of Mechanical Properties for Superalloy K4169; Dissertation, Northwestern Polytechnical University, 2002

[9] Campbell, J.; Castings; Butterworth Heinemann, 2003, ISBN 0750647906

[10] Gottstein, G.; Physical Foundations of Materials Science; Springer Verlag, Berlin, Heidelberg, 2004, ISBN 3540401393